DRAINED FAILURES, STRESS DEPENDENCY AND PLANE STRAIN EFFECTS

Niels Mortensen[1]

KEYWORDS

Plane strain effects and representative friction angles (secant peak values).

ABSTRACT

The bearing capacity factor N_q from Prandtl (1920) was derived for a coarse grained soil, assuming that one friction angle can be used to model the entire range of effective stresses within the rupture figure. A similar rupture figure has been investigated in this paper allowing for stress dependent friction angles throughout the entire failure mechanism using plane and triaxial strain where the friction angle only depends on the density index and on the mean effective stress at failure. To facilitate the continued practical use of the Prandtl solution, the term "representative friction angle" has been introduced and formulas have been established. A representative friction angle will, when used in the work from Prandtl, lead to the same bearing capacity factor or earth pressure coefficient as the stress-dependent model. Differences between plane strain and triaxial strain have been included allowing for establishing factors linking the secant value of a peak friction angle from plane strain to the same parameter in triaxial strain.

1. INTRODUCTION

The scope of this paper is to investigate the effect of using stress dependent friction angles when analysing the traditional solutions for bearing capacity and earth pressures assuming coarse grained materials. The effective strength properties of a coarse grained material will depend on several factors. Given a reasonable homogeneous sand formation characterised by only small variations in the mineralogy and the angularity of the grains, together with the particle size distribution, the secant value of the effective peak friction angle will mainly depend on the density index, I_D, and the effective stress state during failure. This was highlighted by Bolton (1986) who also pointed out that plane strain conditions may increase the shear strength of coarse grained material. Plane strain conditions represents a 3D effective stress state where the intermediate principal strain component (ε_2) is zero as the soil cannot dilate or

[1] Geotechnical Director, nmGeo

contract in the out of plane direction (y-axis on Figure 1, Part 1). The principal effective stress components acting on the slice of soil in part 1 of Figure 1 represents the stress state in the passive Rankine zone ABCA of part 2 of the same figure. The mean effective stress within a soil element is thus dependent on the three principal stress components but since movements in the soil mass can only develop in the XZ-plane the relevant shear stress component will depend on the minor and major principal effective stresses only, $\tau = (\sigma'_1-\sigma'_3)/2$.

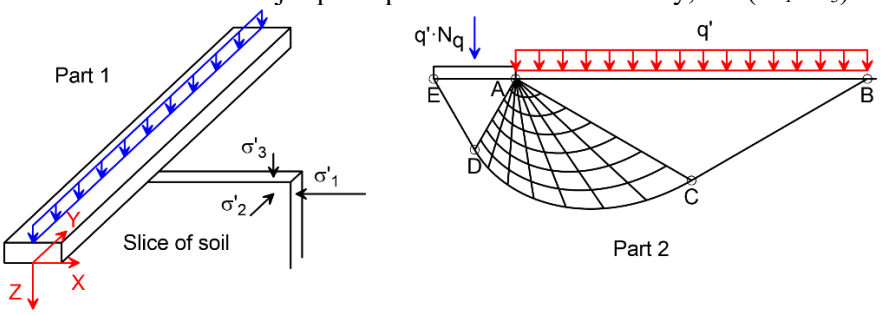

Figure 1 Part 1: 3D view of a strip footing with principal stresses shown on a slice of soil. Part 2: 2D Prandtl rupture figure below a strip footing (surcharge case with zero unit weight and zero effective cohesion).

The symbol φ' represents the secant value of the effective peak friction angle in this paper. The effect of unit weight of soil and the effective cohesion has not been included in this work.

2. A SINGLE SOIL ELEMENT

Basic equations

The secant value of the peak friction angle predicted by Bolton (1986) may be computed by Equations (2.1) through (2.3):

$$\varphi'_{pl} - \varphi'_{cv} = 5 \cdot I_R° \text{ (plane strain)} \quad (2.1)$$

$$\varphi'_{tr} - \varphi'_{cv} = 3 \cdot I_R° \text{ (triaxial strain)} \quad (2.2)$$

$$I_R = I_D \cdot [Q - \log_e(p'_m / 1\text{kPa})] - R < 4.0 \quad (2.3)$$

where φ'_{pl} and φ'_{tr} are secant values of the plane strain and triaxial peak friction angles, respectively, φ'_{cv} is the residual friction angle, I_R is the dilatancy index, p'_m is the mean effective stress at failure, Q is a constant dependent on mineralogy and R = 1.

The value of Q = 10 was proposed for quartz and feldspar sands. Bolton observed a range of 32°-37° for φ'_{cv}, with a mean value of 34° and standard deviation of 2°. The lower end of the interval was dominated by quartz sand, whereas feldspar was found at the upper end. The stress dependency of φ' is introduced through Equation (2.3) where the effective mean stress, p'_m is estimated using:

$$p'_m = (\sigma'_1 + \sigma'_2 + \sigma'_3)/3$$

$$p'_m = \sigma'_3 \cdot [K_{ps} \cdot (1 + b) + 2 - b] / 3 \text{ (Passive failure state)} \quad (2.4)$$

$$p'_m = \sigma'_1 \cdot [1 + b + K_{as} \cdot (2 - b)] / 3 \text{ (Active failure state)}$$

where the principal effective stress components σ'_1, σ'_2 and σ'_3 refer to the state of failure within the sample, $b = (\sigma'_2-\sigma'_3) / (\sigma'_1-\sigma'_3)$ [$b = 0.35$ for plane strain, cf. Lade et al. (2008), and $b = 0$ for triaxial strain] and where K_{ps} and K_{as} are defined in Equation (2.5).

The mean effective stress during failure is estimated differently depending on the failure state (passive or active). The zone ABCA on Figure 1 (Part 2) represents a passive failure state (Rankine zone) where the minor principal effective stress is vertical (σ'_3 = surcharge) for a horizontal soil surface ($\beta = 0$). In an active Rankine zone, the major principal stress is vertical for $\beta = 0$.

The failure criterion for coarse grained materials may be defined by:

$$\sigma'_1/\sigma'_3 = (1+\sin\varphi') / (1 - \sin\varphi') = K_{ps} = 1/K_{as} \quad (2.5)$$

Equations (2.1) through (2.5) form an iterative scheme by which φ'_{pl} or φ'_{tr} can be estimated when φ'_{cv}, I_D, Q and R are known together with one of the principal failure stresses σ'_1 or σ'_3.

The dilatancy index in Equation (2.3) was given a cut off level of 4.0 by Bolton but the value of four may be a conservative value and data have been observed indicating that $I_R < 5$ could be used. Results presented in this paper are generally produced using $Q = 10$, $\varphi'_{cv} = 33°$, $R = 1$ and $b = 0.35$ using a horizontal soil surface combined with a) a vertical wall or b) a horizontal footing.

The parameters Q, R and φ'_{cv} in Equations (2.1) through (2.3) can be calibrated to match site-specific conditions using a few CAD tests (triaxial test being anisotropically consolidated and sheared drained).

Plane strain factor, single soil element

The plane strain factor is defined as the ratio between the secant value of the plane strain peak friction angle and the same parameter in triaxial strain, $\varphi'_{pl}/\varphi'_{tr}$. Figure 2 left illustrates the plane strain factor for single soil elements using Bolton (1986) following the basic equations above.

The curves for the active stress state refer to a major effective principal stress being vertical, while the vertical effective stress is taken as the minor principal effective stress for the passive case. Figure 2 left shows a) The plane strain factor for a single soil element increases with the density index and decreases for increasing mean effective stress. The active failure state reveals a higher factor than the passive failure state. b) The dilatancy index increases for decreasing mean effective stress. Values of I_R of 4 and 5 are illustrated on Figure 2 left (curves are not drawn for $I_R > 5$).

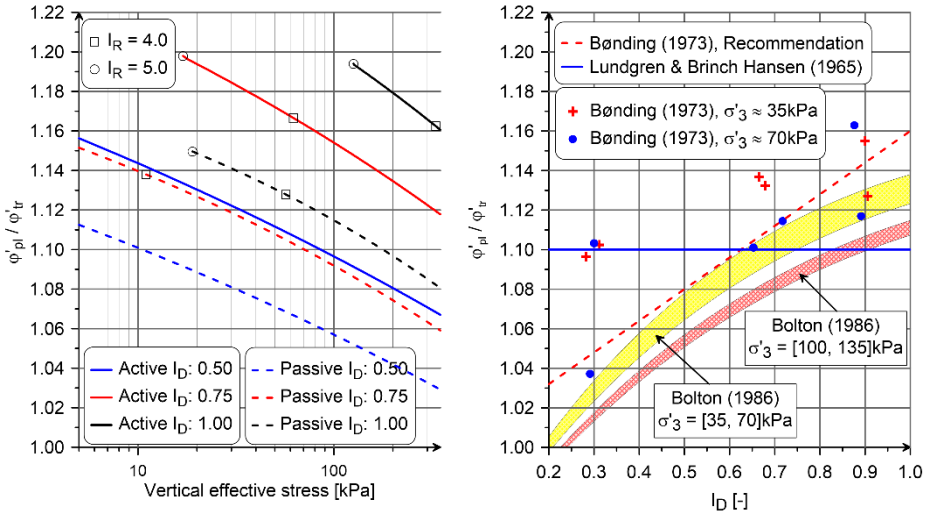

Figure 2 Plane strain factor versus [Left: vertical effective stress for active and passive failure states] and [Right: density index].

The plane strain factor is not strongly linked to the value of $b = (\sigma'_2-\sigma'_3)/(\sigma'_1-\sigma'_3)$. Using b = 0.20 and 0.40 implies a plane strain factor decreasing from 1.192 to 1.182 for an active failure and from 1.125 to 1.117 for a passive failure assuming I_D = 0.75 and a vertical effective stress of 30kPa.

Bønding (1973) used the results from 12 triaxial and 12 plane strain compression tests to recommend $\varphi'_{pl} = \varphi'_{tr}\cdot(1+0.16\cdot I_D)$ as shown as the dashed red line in Figure 2 right, but recommended further testing to support this hypothesis. Lundgren and Brinch Hansen (1965) suggested to use a plane strain friction angle being 10% higher than φ'_{tr} with no dependency of the density index and with no data provided to support this conclusion (blue line in Figure 2 right). It is the dilatancy that causes the plane strain factor, so Lundgren & Brinch Hansen (1965) should not be used, cf. also Steenfelt (2004). The yellow filled area on Figure 2 right represents the range of the plane strain factor (passive) using Bolton (1986) with σ'_3 = 35-70kPa (stress range identical to Bønding (1973)). The red filled area represents an identical approach but using σ'_3 between 100 and 135kPa. It is seen that the recommendation from Bønding (1973) [$\varphi'_{pl} = \varphi'_{tr}\cdot(1+0.16\cdot I_D)$] is an unsafe approximation to the Bolton interval with σ'_3 between 35 and 70kPa and that higher (but still realistic) values of σ'_3 may reduce the plane strain factor further. It is indicated by Figure 2 right that a safer approximation accounting for larger mean effective stresses could be $\varphi'_{pl} = \varphi'_{tr}\cdot(1+0.10\cdot I_D)$, which is the expression included in EN 1997-1 DK NA:2021.

3. RELATIVE DENSITY INDEX

The x-axis on Figure 2 right refer to the density index I_D, which is defined by $I_D = \gamma_{d,max} \cdot (\gamma_{d,i} - \gamma_{d,min}) / [\gamma_{d,i} \cdot (\gamma_{d,max} - \gamma_{d,min})]$ and where $\gamma_{d,max}$ and $\gamma_{d,min}$ are the maximum and minimum dry total unit weights, respectively, and $\gamma_{d,i}$ is the dry in-situ unit weight. Different standards exist for determining the minimum and maximum dry densities and these standards will usually lead to approximately the same value of the minimum dry density, but they will often lead to a significant scatter in the measured maximum dry density and the value of the density index is thus an ambiguous parameter. The subject about density index was investigated in Lunne et al. (2019) reaching the conclusion: *Therefore, it is concluded that there is a need for the development of new standards for a robust determination of $\gamma_{d,max}$ and $\gamma_{d,min}$ values. Specifically, a standard for determining $\gamma_{d,max}$ is required to consistently obtain results at the upper bound of dry unit weight values for the likely range of sands — without crushing the sand grains.*

Knudsen et al. (2020) followed up on the work from Lunne et al. (2019) arriving at a new procedure for identifying the maximum and minimum dry density. It was found that if the suggested approach was followed, different laboratories and different operators within the same laboratory would arrive at almost identical values of the maximum and minimum dry density. The density index has in this paper been used a unique number and with the new method from Knudsen et al. (2020) this approach seems reasonable.

As the challenge with measuring $\gamma_{d,max}$ unambiguously is solved, one of the main outstanding issues on the laboratory side is to establish a practice for reconstituting sand samples for advanced laboratory testing. The author of this paper was running a laboratory program for a wind farm involving three different geotechnical laboratories with their individual reconstitution procedures. Each laboratory was given an identical sand batch for running two CADc tests using the same $\gamma_{d,max}$ and $\gamma_{d,min}$ provided by the Client. One laboratory could reproduce the peak friction angle with an accuracy of 0.5° when comparing the two tests while the reproducibility for the two remaining laboratories was 2-3°. A difference of more than 10° was observed when comparing the mean value of the friction angle from the different laboratories and these observations highlight the need of an international standard for reconstituting of coarse grained samples in the laboratory.

4. STRESS DEPENDENT MODELS

Introduction

The traditional estimates of either earth pressures or bearing capacities are usually based on closed form expressions defining an earth pressure coefficient or a bearing capacity factor.

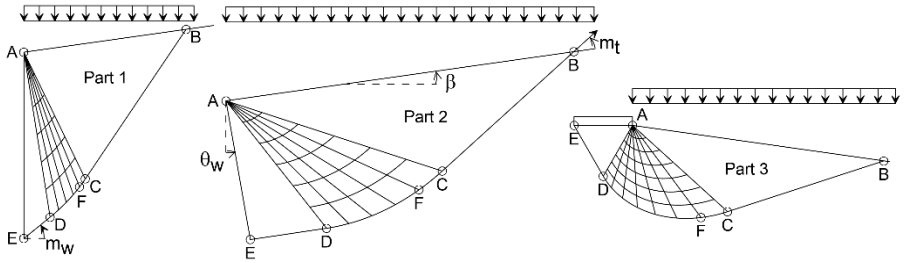

Figure 3 Examples of traditional rupture figures for vertical bearing capacity and lateral earth pressure. Part 1: Active earth pressure, Part 2: Passive earth pressure and Part 3: Bearing capacity.

ABCA on Figure 3 represents a Rankine zone spanned by straight lines and where the mean effective stress within the zone is constant. The zone ACDA is a Prandtl-zone composed of logarithmic spiral arcs and where the mean effective stress increases as the radius in the logarithmic spiral decreases. A stiff soil body ADEA is observed near the wall / footing, and the mean effective stress is constant inside this zone.

The soil surface may be inclined β with horizontal while the wall may be inclined θ_w with vertical. At point B the bounding rupture line forms an angle with the soil surface of m_t, and the angle at point E between the normal to the wall proper and the bounding rupture line is called m_w.

The rupture figures on Figure 3 are based on one friction angle, used to model the full range of effective stress states. The geotechnical engineer must therefore decide upon a relevant effective stress level reflecting "a representative friction angle" that covers the variation in mean effective stress (and friction angle) throughout the rupture figure in question and this paper will suggest some guidelines as to how this can be performed. The models included in the work are based on zone ruptures only, cf. Figure 3.

Theoretical basis

A brief description of the theory applied is given below. The reader is referred to either Hansen (2001) or Mortensen & Krogsbøll (2019) for more details. All equations refer to statically admissible rupture mechanisms that are also kinematically admissible when assuming associated flow. The minor principal effective stress within ABCA is estimated by:

$$\sigma'_3 = \frac{q \cdot \cos^2\beta \cdot (1-\sin\varphi')}{1-\sin\varphi' \cdot \sin(2m_t+\varphi')} \qquad (4.1)$$

where m_t can be found by $\cos(2 \cdot m_t+\varphi'+\beta) = -\sin\beta/\sin\varphi'$ and φ' is computed by Bolton (1986). The effective stress state and the friction angle varies throughout the Prandtl-zone, which is divided into a series of slices each spanning an angle α of ~1°. Assume that point F is the neighbouring point to C along CD (cf. Figure 3), the minor principal effective stress at point F can

then be computed from $\sigma'_{3,F} = \sigma'_{3,C} \cdot \exp(2 \cdot \alpha \cdot \tan[0.5 \cdot (\varphi'_C + \varphi'_F)])$ representing an iterative procedure. The bounding rupture line at point C is inclined $m_C = \beta + m_t$ with horizontal while $m_F = m_C - \alpha$. The Prandtl-zone can be analysed by this procedure and the result is the minor principal effective stress at point D together with the angle m_D. The angle at point D needs for statically reasons to be $m_D = m_w + \theta_w$ (both symbols shown on Figure 3) for earth pressure problems where m_w is computed by $\cos(2 \cdot m_w + \varphi'_D + \delta) = \sin\delta / \sin\varphi'_D$ (δ is the interface friction angle of the wall). For the bearing capacity problem (Figure 3 Part 3) the value of $m_D = -(\pi/4 + \varphi'_D/2)$ representing the angle of the rupture line at point D being identical to the angle at point E. The stress dependent bearing capacity factor, $N_{q,st}$ and the stress dependent earth pressure coefficient, $K_{q,st}$ can then be computed from the estimated values of φ'_D and m_D:

$$q \cdot N_{q,st} = \left(\sigma'_{1,D} + \sigma'_{3,D}\right) \cdot [1 + sin\varphi'_D]/2 \tag{4.2}$$

$$q \cdot K_{q,st} = \left(\sigma'_{1,D} + \sigma'_{3,D}\right) \cdot [1 + sin\varphi'_D \, sin(2m_w + \varphi'_D)]/2 \tag{4.3}$$

The value of $\sigma'_{1,D}$ can be found from Equation (2.5). Each slice in the Prandtl zone spans 1° and if this value is replaced by 5° the results presented will not change.

Computed variations of the friction angle

The variation of the friction angle modelled using the theoretical basis is shown in Figure 4 assuming plane strain conditions and a surcharge of 20kPa for the cases bearing capacity, active pressure and passive pressure. The red curve represents $I_D = 0.60$ for passive and bearing capacity while the blue curve reflects $I_D = 0.90$ for the same cases. The black curve is an active earth pressure using $I_D = 0.60$.

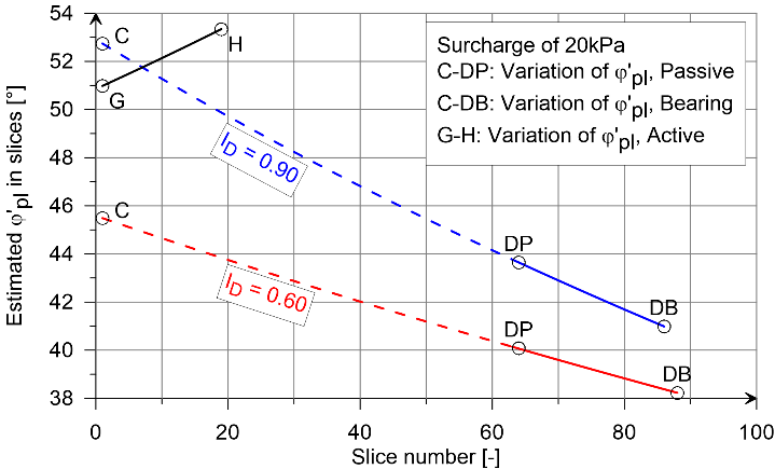

Figure 4 Estimated plane strain friction angle in the slices, where slice number 1 represents point C on Figure 3 and where the highest slice number refer to point D.

The dashed blue curve (I_D = 0.90) between C and DP is the estimated friction angles within the Prandtl-zone for the passive earth pressure case, showing ~9° variation in φ_{pl}' caused by variation in the mean effective stress. The blue curve between C and DB is the variation within the bearing capacity case showing ~12° variation in φ_{pl}'. The red curve (I_D = 0.60) in Figure 4 show variations between ~6° and ~8° for the same cases. The black curve between G and H is the active case (I_D = 0.60) with only small variations in φ'.

Representative friction angles

The equation for the bearing capacity factor N_q for an isotropic homogeneous soil is shown in several textbooks, e.g. Hansen (2001):

$$N_q = \frac{1+sin\,\varphi'}{1-sin\,\varphi'} e^{2\alpha\, tan\,\varphi'} \qquad (4.4)$$

where $\alpha = m_t - m_w + \beta - \theta_w$ (leading to $\alpha = \pi/2$ for $\beta = 0$). The corresponding earth pressure coefficient is:

$$K_q = cos^2\beta \frac{1+sin\,\varphi'\,sin(2m_w+\varphi')}{1-sin\,\varphi'\,sin(2mt+\varphi')} e^{2\alpha\, tan\,\varphi'} \qquad (4.5)$$

The representative friction angle is defined as the friction angle to use in Equation (4.4) to match the result from Equation (4.2) and similar using (4.5) and (4.3). The intention with this approach is to establish a frame to use when deriving the representative friction angle for a practical design and where the selected friction angle accounts for variations in the effective stresses within the rupture figure in question.

For a bearing capacity case Figure 4 reveals that the maximum friction angle, φ'_{max} is found at point C in Figure 3 and that the friction angle decreases almost linearly towards point DB where φ'_{min} is found. Studying the effect of a series of different variations in the surcharge and the density index leads to the following simplification for the bearing capacity case:

$$\varphi'_{rep} = 0.5 \cdot \left(\varphi'_{max} + \varphi'_{min}\right) \qquad (4.6)$$

The value of φ'_{max} refer to the zone ABCA in Figure 3, Part 3, and it can be computed directly (σ'_3 = surcharge) following Bolton (1986) and φ'_{min} can be found in a similar way for the zone ADEA provided that a reasonable estimate of the bearing capacity is known (σ'_1 = bearing capacity). The value of φ'_{rep} from Equation (4.6) can be used in Equation (4.4) to absorb the effect of variations in the effective mean stress within the rupture figure. Estimating φ'_{rep} from $N_q = N_{q,st}$ and comparing with the results from Equation (4.6) implies a difference in φ'_{rep} of less than 0.1° for both plane strain and triaxial strain.

Considering the passive earth pressure case, a similar approach as shown in Equation (4.6) may be given where the maximum friction angle is found in the same zone as found for the bearing capacity case. However, the minimum

friction angle in the passive case is found in a zone where the principal effective stress directions vary with the relative roughness of the wall and simple procedures may therefore not be established referring to both φ'_{min} and φ'_{max}. Considering a series of different variations in the surcharge and the density index leads to the following simplification for the passive earth pressure case:

$$\varphi'_{rep} = \varphi'_{max} - A \cdot I_D \cdot \sqrt{tan\delta / tan\varphi'} \qquad (4.7)$$

The factor "A" in Equation (4.7) equals 2.1 for triaxial strain and 4.0 for plane strain. The accuracy of the results from Equation (4.7) can be evaluated by comparing with the result obtained using $K_q = K_{q,st}$ and Equation (4.7) will imply results within ±0.2° for triaxial strain and ±0.5° for plane strain with the A-factors given. Considering the active earth pressure cases, Figure 4 indicates that the difference between φ'_{max} and φ'_{min} is small and that φ'_{min} is found in the zone ABCA in Figure 3. It is therefore suggested that $\varphi'_{rep} = \varphi'_{min}$ for the active case.

5. PLANE STRAIN FACTOR, STRUCTURES

Figure 5 shows the plane strain factor, defined as the representative friction angle for plane strain conditions divided by the representative friction angle for triaxial strain conditions, for the failure types from Figure 3.

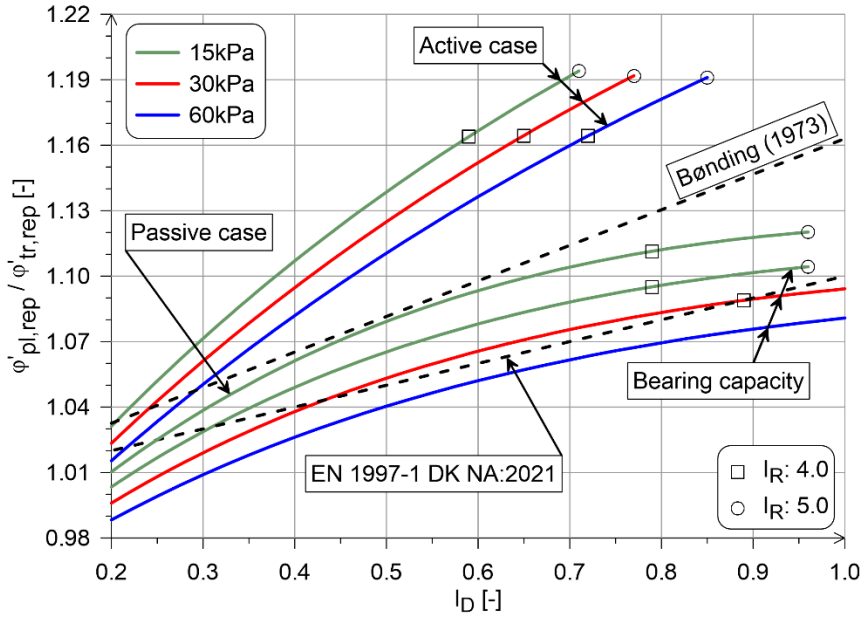

Figure 5 Plane strain factor versus density index for a bearing capacity case, an active case and for a passive case using different values of the surcharge. The earth pressure cases are based on tanδ/tanφ' = 2/3.

The individual curves on Figure 5 represent the combined effect of merging a series of stress dependent soil elements into one plane strain factor being dependent on the density index.

Different colour codes on Figure 5 represent different values of the applied surcharge where 15kPa, 30kPa and 60kPa have been used for the active case and the bearing capacity. The passive case is only computed for 15kPa. The earth pressure cases are computed using $\tan\delta/\tan\varphi' = 2/3$. The recommendation from Bønding (1973) and from EN 1997-1 DK NA:2021 are illustrated through black dashed lines and symbols are included to represent the location of I_R of 4.0 and 5.0. The 15kPa passive case is seen to deviate only marginally from the 15kPa bearing capacity case so the passive case and the bearing capacity curves are almost identical (at least for a relative roughness of 0.6 or higher). A smooth wall in passive earth pressure implies a plane strain factor of 1.15 for $I_D = 0.90$ and 15kPa surcharge, which is identical to the recommendation from Bønding (1973) and which exceeds the corresponding factor from bearing capacity by 0.05.

The estimates forming the background for Figures 5 do not include the effect of the unit weight of soil (or the effective cohesion) and this will cause the mean effective stress to be computed too low, implying that the estimated plane strain factor may be on the high side. Most footings gain their main capacity part from the overburden pressure at foundation level so the practical use of Figure 5 would likely call for the surcharge load in nature to be used as a guideline for selecting the plane strain factor from Figure 5. The conservatism in the approach from EN 1997-1 DK NA:2021 should compensate for the possible effect of using a too low effective mean stress level.

The representative surcharge load for the active and the passive case should likely be the vertical effective in-situ stress halfway down the embedded part of the wall when Figure 5 is used in a design case. This recommendation is based on engineering judgement to compensate for an increasing effective overburden pressure in the nature, which is not included in the estimates behind Figure 5. This recommendation should be on the safe side knowing that EN 1997-1 DK NA: 2021 do not allow utilizing higher plane strain factors than shown as the dashed line in Figure 5. The robustness in a sheet pile wall design is mainly controlled by the relative roughness of the front side of the wall (combined with the applied differential water pressure).

6. CONCLUSIONS

When stress-dependent friction angles are accounted for in the traditional rupture mechanisms for vertical bearing capacity and lateral earth pressures, the corresponding coefficients will change. Simple equations are proposed in this paper to ensure that one representative friction angle may be extracted and

used in these classical expressions to compensate for variations of approximately 10° in the estimated value of φ' within the rupture figures.

Differences between plane strain friction angles and friction angles assuming triaxial strain are studied. The plane strain factor is defined as the factor to multiply on φ'_{tr} to estimate φ'_{pl}. The factor will depend on the effective mean stress, the density index, and the type of failure in question. EN 1997-1 DK NA:2021 allows for using this effect but results from this paper indicates that the plane strain factor is not fully utilized in EN 1997-1 DK NA:2021.

It is pointed out that the geotechnical community is short of an international standard considering reconstitution of samples of coarse grained material in the geotechnical laboratory.

Bønding (1973), Bolton (1986) and Andersen & Schjetne (2013) seems to align on the subject about triaxial friction angles and the dependency with effective stresses during failure and density index. Furthermore, Bønding (1973) and Bolton (1986) seems to find resembling values for the secant value of the peak friction angle in plane strain. In this way the basis for the present paper seems to be reasonably confirmed when work from other sources than Bolton (1986) is included.

This paper indicates that the shear strength of coarse grained material is significantly higher than what is usually used in Denmark. A high utilization of the shear strength calls for increased focus on the effect of dilatancy when deriving parameters for models following associated or non-associated flow. This subject has been touched in Mortensen & Steenfelt (2024).

More plane strain testing should be conducted on commercial projects.

ACKNOWLEDGEMENT

Dr. Anette Krogsbøll has reviewed the paper with corresponding equations, and she has made valuable comments to improve readability. Her efforts are highly appreciated.

REFERENCES

Andersen K.H. & Schjetne K. (2013). Database of Friction Angles of Sand ad Consolidation Characteristics of Sand, Silt and Clay, Journal of Geotechnical and Geoenvironmental Engineering, ASCE, July 2013, pp. 1140-1155.

Bolton M.D. (1986). The strength and dilatancy of sands, Geotechnique 36, No. 1, pp. 65-87.

Bønding N. (1973). A true triaxial failure criterion in sand (Ph.D.-Thesis in Danish), Technical University of Denmark, Copenhagen, 1973 (Also published in DGI-Bulletin 30).

Hansen B. (2001). Advanced Theoretical Soil Mechanics, Dgf-Bulletin 20, ISBN 87-89833-11-2.

Knudsen S., Powel, J.J.M., Lunne, T., Thomsen N.V., Krogh, L. and Barwise, A. (2020). Development of New Robust Procedures for the Determination of Maximum and Minimum Dry Densities of Sand, 4th International Symposium on Frontiers in Offshore Geotechnics. Proceedings. (ISFOG).

Lade P.V., Nam J. & Hong W.P. (2008). Shear banding and cross-anisotropic behaviour observed in laboratory sand tests with stress rotation. Canadian Geotechnical Journal, 2008, Volume 45, pp. 74-84.

Lundgren H. & Brinch Hansen J. (1965). Geoteknik (Geotechnics in Danish), Teknisk Forlag, Copenhagen 1965.

Lunne T., Knudsen S., Blaker Ø., Vestgaarden T., Powell J.J.M., Wallace C.F., Krogh L., Thomsen N.V., Yetgniner G. & Ghanekar R.K. (2019). Methods used to determine maximum and minimum dry unit weights of sand: Is there a need for a new standard? Canadian Geotechnical Journal 2019. Volume 56, pp. 536-553.

Mortensen N. & Krogsbøll A. (2019). Effect of tangential surface load components on earth pressure coefficients, Proceedings of the XVII ECSMGE 2019.

Mortensen N. & Steenfelt J.S. (2024). L-shaped gravity walls. Recommended practice for ULS. 19th Nordic Geotechnical Meeting, Göteborg 2024.

Prandtl L. (1920), Über die Härte plastischer Körper., Nachr. D. Ges. D. Wiss., math-phys. Kl., Göttingen 1920.

Steenfelt J.S. (2004), Guestimate of φ', c' and ψ for coarse grained soil, NGM 2004, XIV Nordic Geotechnical Meeting, May 19th – 21st, 2004, Proceedings Volume 1.